

1 **Biallelic mutation of *CLRN2* causes non-syndromic hearing loss in**
2 **humans**

3
4 Barbara Vona^{1,2}, Neda Mazaheri^{3*}, Sheng-Jia Lin^{4*}, Lucy A Dunbar^{5*}, Reza Maroofian⁶,
5 Hela Azaiez⁷, Kevin T. Booth^{7,8}, Sandrine Vitry⁹, Aboufazi Rad², Pratihtha Varshney⁴,
6 Ben Fowler¹⁰, Kumar N. Alagramam^{11,12,13}, David Murphy⁶, Gholamreza Shariati^{14,15},
7 Alireza Sedaghat¹⁶, Henry Houlden⁶, Shruthi VijayKumar⁴, Richard J. H. Smith⁷,
8 Thomas Haaf¹, Aziz El-Amraoui⁹, Michael R. Bowl^{5,17**}, Gaurav K. Varshney^{4**}, Hamid
9 Galehdari^{3**}

10 *These authors contributed equally

11 **These authors contributed equally

12 ¹Institute of Human Genetics, Julius Maximilians University Würzburg, Würzburg,
13 Germany

14 ²Department of Otolaryngology—Head and Neck Surgery, Tübingen Hearing Research
15 Centre, Eberhard Karls University Tübingen, Tübingen, Germany

16 ³Department of Genetics, Faculty of Science, Shahid Chamran University of Ahvaz,
17 Ahvaz, Iran

18 ⁴Genes & Human Disease Research Program, Oklahoma Medical Research
19 Foundation, Oklahoma City, OK, United States

20 ⁵Mammalian Genetics Unit, MRC Harwell Institute, Harwell Campus, OX11 0RD, UK

21 ⁶Department of Neuromuscular Disorders, UCL Queen Square Institute of Neurology,
22 London, WC1N 3BG, UK

23 ⁷Molecular Otolaryngology and Renal Research Laboratories, Department of
24 Otolaryngology and Interdisciplinary Graduate Program in Molecular Medicine, Carver
25 College of Medicine, University of Iowa, Iowa City, IA, USA

26 ⁸Harvard Medical School, Department of Neurobiology, Boston Massachusetts

27 ⁹Unit Progressive Sensory Disorders, Pathophysiology and Therapy Institut Pasteur,
28 Institut de l'Audition, INSERM-UMRS1120, Sorbonne Université, 63 rue de Charenton,
29 75012 Paris, France

30 ¹⁰Imaging & Histology Core, Oklahoma Medical Research Foundation, Oklahoma City,
31 OK, United States

32 ¹¹Department of Otolaryngology, University Hospitals Cleveland Medical Center, School
33 of Medicine, Case Western Reserve University, 11100 Euclid Avenue, Cleveland, Ohio,
34 44106, USA

35 ¹²Department of Neurosciences, Case Western Reserve University, 11100 Euclid
36 Avenue, Cleveland, Ohio, 44106, USA

37 ¹³Department of Genetics and Genomic Sciences, Case Western Reserve University,
38 Cleveland, Ohio 44106, USA

39 ¹⁴Department of Medical Genetics, Faculty of Medicine, Ahvaz Jundishapur, University
40 of Medical Sciences, Ahvaz, Iran

41 ¹⁵Narges Medical Genetics and Prenatal Diagnostics Laboratory, East Mihan Ave.,
42 Kianpars, Ahvaz, Iran

43 ¹⁶Diabetes Research Center, Health Research Institute, Ahvaz Jundishapur University
44 of Medical Sciences, Ahvaz, Iran

45 ¹⁷UCL Ear Institute, University College London, 332 Gray's Inn Road, WC1X 8EE,
46 London, UK

47

48 Correspondence:

49 Barbara Vona : Email: barbara.vona@uni-wuerzburg.de, Tel: +49 (0)931-31-84244

50 Current Email: barbara.vona@uni-tuebingen.de, Tel: +49 (0)7071-29-88154

51 Michael R. Bowl: Email: m.bowl@har.mrc.ac.uk, Tel: +44 (0)1235 841161

52 **Disclosure**

53 The authors declare no conflict of interest.

54 **Abstract**

55 Deafness, the most frequent sensory deficit in humans, is extremely heterogenous with
56 hundreds of genes probably involved. Clinical and genetic analyses of an extended
57 consanguineous family with pre-lingual, moderate-to-profound autosomal recessive
58 sensorineural hearing loss, allowed us to identify *CLRN2*, encoding a tetraspan protein
59 as a new deafness gene. Homozygosity mapping followed by exome sequencing
60 identified a 15.2 Mb locus on chromosome 4p15.32p15.1 containing a missense
61 pathogenic variant in *CLRN2* (c.494C>A, NM_001079827.2) segregating with the
62 disease. Using *in vitro* RNA splicing analysis, we show that the *CLRN2* c.494C>A
63 mutation leads to two events: 1) the substitution of a highly conserved threonine
64 (uncharged amino acid) to lysine (charged amino acid) at position 165, p.(Thr165Lys),
65 and 2) aberrant splicing, with the retention of intron 2 resulting in a stop codon after 26
66 additional amino acids, p.(Gly146Lysfs*26). Expression studies and phenotyping of
67 newly produced zebrafish and mouse models deficient for clarin 2 further confirm that
68 clarin 2, expressed in the inner ear hair cells, is essential for normal organization and
69 maintenance of the auditory hair bundles, and for hearing function. Together, our
70 findings identify *CLRN2* as a new deafness gene, which will impact future diagnosis and
71 treatment for deaf patients.

72

73 **Keywords:** autosomal recessive hearing loss (DFNB), clarin 2 (*CLRN2*); deafness;
74 homozygosity mapping; non-syndromic hearing loss

75 **Introduction**

76 The mammalian inner ear is an exquisite and highly complex organ, made up of
77 the vestibule, the organ responsible for balance, and the cochlea, the sensory organ for
78 hearing. The auditory sensory cells of the inner ear are called the inner and outer hair
79 cells that are responsible for transduction of sound wave-induced mechanical energy
80 into neuronal signals (Gillespie and Müller, 2009; Hudspeth, 1997). The functional
81 mechanoelectrical transduction machinery involves intact formation and maintenance of
82 a highly specialized and organized structure, the hair bundle. The hair bundle contains a
83 few dozen F-actin-filled stereocilia, arranged in a highly interconnected and highly
84 organized staircase-like pattern, which is critical for function (Kazmierczak et al., 2007).
85 Knowledge of the mechanisms of formation, maintenance, and function of the
86 transduction complex is limited (Cunningham and Müller, 2019). In this regard,
87 identification of novel genes that encode protein products essential for hearing is likely
88 to improve our understanding of the physical, morphological and molecular properties of
89 hair cells and associated mechanistic processes.

90 Hereditary hearing loss is one of the most common and genetically
91 heterogeneous disorders in humans (Wright et al., 2018). Sensorineural hearing loss
92 has an incidence of one to two per 1000 at birth (Morton and Nance, 2006). It displays
93 extraordinary phenotypic, genetic and allelic heterogeneity, with up to 1,000 different
94 genes potentially involved (Ingham et al., 2019). So far, about 120 genes and more than
95 6,000 disease causing variants (Azaiez et al., 2018) have been identified as responsible
96 for non-syndromic hearing loss in humans (see <http://hereditaryhearingloss.org/> and
97 <http://deafnessvariationdatabase.org/>), and many more are yet to be discovered.

98 Genetic factors predominate the etiological spectrum and most of hereditary hearing
99 loss appears to follow an autosomal recessive inheritance pattern (Smith et al., 2005).
100 Approximately 80% of the currently known autosomal recessive genes have been
101 identified by studying extended consanguineous families (Hofrichter et al., 2018). There
102 are many forms of hearing loss that are clinically indistinguishable but caused by distinct
103 genetic entities that are presently unknown. Identification of additional genes essential
104 for auditory function, through the study of families exhibiting hereditary hearing loss, will
105 not only help increase our understanding of the biology of hearing, but will also identify
106 new molecular targets for therapeutic intervention.

107 Through the study of an extended consanguineous Iranian family, we have
108 identified a *CLRN2* coding lesion as the cause of hearing loss in family members that
109 are homozygous for the allele. We have established that clarin 2 likely plays a critical
110 role in mechanotransducing stereocilia of the hair bundle in zebrafish and mouse.
111 *CLRN2* belongs to the clarin (CLRN) family of proteins that are comprised of three
112 orthologues named clarin 1, 2, and 3 that encode four-transmembrane domain proteins.
113 Pathogenic variants in *CLRN1* (clarin 1) cause either non-syndromic retinitis
114 pigmentosa (RP) (Khan et al., 2011) or Usher syndrome type 3A (USH3A), that is
115 characterized by progressive hearing loss, RP and variable vestibular dysfunction
116 (Adato et al., 2002; Joensuu et al., 2001; Ness et al., 2003; Plantinga et al., 2005). This
117 study establishes clarin 2 as essential for inner ear function in zebrafish, mice and
118 humans, with a loss-of-function allele leading to autosomal recessive non-syndromic
119 sensorineural hearing loss (ARNSHL).

120 **Materials and Methods**

121 **Patient clinical and audiometry data**

122 A three generation Iranian family of Lurs ethnicity was ascertained as part of a
123 large ethnically diverse Iranian population rare disease study. After obtaining written
124 informed consent from all participants with approval by the Faculty of Medicine ethics
125 commissions at the University of Würzburg (46/15) and Shahid Chamran University of
126 Ahvaz (#EE/97.24.3 17654), pure-tone audiograms and medical information were
127 collected from participating members. Clinical examination excluded additional
128 syndromic features.

129 Individuals IV-1, IV-6, and V-1 (Figure 1) underwent complete ear, nose and
130 throat examination, including binocular ear microscopy and external ear inspection.
131 Routine pure-tone audiometry was performed according to current standards that
132 measured hearing thresholds at frequencies 0.25, 0.5, 1, 2, 4, 6 and 8 kHz. Both air-
133 and bone-conduction thresholds were determined. Severity of hearing loss was defined
134 as previously described (Mazzoli et al., 2003). Individuals IV-1 and IV-6 underwent
135 additional tympanometry and speech recognition threshold testing. Audiometry testing
136 for individuals IV-1, IV-6, and V-1 was performed at ages 29 years, 44 years, and 20
137 years, respectively.

138 **Genotyping, homozygosity mapping, copy number variation and exome** 139 **sequencing data analyses**

140 Due to parental consanguinity and suspected autosomal recessive mode of
141 inheritance, we assumed that the causative variant would be homozygous and identical

142 by descent in affected individuals in the fourth generation of the family. Blood samples
143 from 14 family members were obtained and genomic DNA was isolated from whole
144 blood using standard procedures. DNA from affected (IV-1, IV-6, and IV-8) and
145 unaffected (IV-2, IV-3, IV-4, and IV-5) individuals were genotyped using the Infinium
146 Global Screening Array-24 v1.0 BeadChip (Illumina, San Diego, CA, USA) according to
147 manufacturer's protocols. Homozygosity mapping was performed using Homozygosity
148 Mapper to identify common homozygous intervals among the affected individuals
149 (Seelow et al., 2009). Runs of homozygosity with a maximum threshold of 0.99 were
150 checked after the exome-wide analysis was completed. Copy number variation calling
151 was performed using GenomeStudio v.2011.1 and cnvPartition 3.2.0 (Illumina).

152 For exome sequencing, DNA samples from two affected individuals (IV-1 and IV-
153 6) were used. The data from individual IV-6 was analyzed exome-wide and data from
154 individual IV-1 was used for determination of allele sharing. Exome capture using
155 genomic DNA was performed using the SureSelect Target Enrichment v6 (Agilent) kit
156 following manufacturer's recommendations. The libraries were sequenced with a
157 HiSeq4000 (Illumina). Data analysis was performed using the Burrows-Wheeler
158 Alignment (BWA) tool for read mapping to the human reference genome GRCh37
159 (hg19), Picard for duplicate removal, GATK for local re-alignment, base recalibration,
160 variant calling, and variant annotation, and SnpEff for variant annotation. Variant filtering
161 was based on: coverage > 10X, Phred quality score ≥ 30 , and minor allele frequency
162 (MAF) ≤ 0.005 as reported in 1000 Genomes Project and EVS6500. Variants were
163 filtered based on coding effect (non-synonymous, indels, and splice site variants), and
164 artifact-prone genes (*HLAs*, *MAGEs*, *MUCs*, *NBPFs*, *ORs*, *PRAMEs*) were excluded.

165 Visualization was performed using the Integrative Genomics Viewer. Analysis of
166 homozygous and compound heterozygous variants between the two sequenced
167 affected individuals (IV-6 and IV-1) followed. We analyzed missense variants by using a
168 combination of criteria that scored conservation using GERP++ and PhyloP, and
169 deleterious or pathogenic scores in Combined Annotation Dependent Depletion (CADD)
170 (Kircher et al., 2014), LRT (Chun and Fay, 2009), MutationTaster (Schwarz et al.,
171 2014), PolyPhen-2 (Adzhubei et al., 2010), and SIFT (Ng and Henikoff, 2001). Missense
172 variants were excluded when three out of five *in silico* pathogenicity prediction tools
173 yielded a benign score. Manual MAF analysis used gnomAD (Lek et al., 2016), GME
174 (Scott et al., 2016), and Iranome (Fattahi et al., 2019). Potential effects on splicing were
175 assessed using ESEfinder (Cartegni et al., 2003) and RESCUE-ESE (Fairbrother et al.,
176 2004).

177 **Segregation, sequence and *in vitro* splicing analyses of the *CLRN2* c.494C>A** 178 **pathogenic variant**

179 To confirm segregation of the *CLRN2* c.494C>A; p.(Thr165Lys)
180 (NM_001079827.2) homozygous variant, Sanger sequencing was completed in all 14
181 family members using the following primers (*CLRN2* Ex3 F: 5'-
182 AAATGCCACCTCTTACAGAGTTGC-3' and *CLRN2* Ex3 R: 5'-
183 ACCGTGGCCTCTTCGATTTTGGTC-3') and standard PCR and sequencing
184 parameters.

185 To document residue conservation, CLRN1 (UniProt: P58418) and CLRN2
186 (UniProt: A0PK11) were aligned and visualized in Jalview (Waterhouse et al., 2009)
187 with an overview of the pathogenic and likely pathogenic missense and nonsense

188 *CLRN1* variants retrieved from the Deafness Variation Database v 8.2 (Azaiez et al.,
189 2018).

190 In addition, secondary protein structure prediction of human CLRN2
191 (NP_001073296.1) that included the wild-type (WT) and mutated amino acid residues
192 was performed using I-TASSER (Yang et al., 2015).

193 To assess the splicing effect of the c.494C>A variant, *in vitro* splicing assays,
194 also called mini-genes, were carried out as described (Booth et al., 2018a; Booth et al.,
195 2018b). Concurrently, the mini-gene splice assay experiment was conducted in a
196 double-blind manner as previously described (Lekszas et al., 2020). A detailed
197 description of this method can be found in the Supplementary Methods.

198 **CRISPR/Cas9-mediated inactivation of *clrn2* in zebrafish**

199 Zebrafish (*Danio rerio*) were raised and maintained in an AALAC accredited
200 facility at the Oklahoma Medical Research Foundation (OMRF) under standard
201 conditions. Zebrafish embryos/larvae were maintained in embryo medium with
202 0.00002% methylene blue and raised at 28°C. All animal experiments were performed
203 as per protocol (17-01) and approved by the Institutional Animal Care Committee of
204 OMRF (IACUC). All zebrafish handling, embryo care, and microinjections were
205 performed as previously described (Westerfield, 2000). WT zebrafish strain NHGRI-1
206 was used for all experiments (LaFave et al., 2014). The zebrafish embryonic staging
207 was determined by morphological features according to Kimmel et al (Kimmel et al.,
208 1995).

209 To produce zebrafish *clrn2* crispants, the sgRNA target sequences were selected
210 from the UCSC genome browser tracks generated by the Burgess lab. Five

211 independent targets were chosen and sgRNAs were synthesized by *in vitro* transcription
212 as described earlier (Varshney et al., 2016). sgRNAs and Cas9 protein complex were
213 used to generate indels. A 6 μ L mixture containing 2 μ L of 40 μ M Spy Cas9 NLS protein
214 (New England Biolabs, MA, USA), 200 ng each of five sgRNAs (in 2 μ L) and 2 μ L of 1
215 M potassium chloride was injected into one-cell-stage WT embryos. Injection volumes
216 were calibrated to 1.4 nL per injection. Insertion/deletion (indel) variants were detected
217 by amplifying the target region by PCR and Sanger sequencing as described earlier
218 (Varshney et al., 2016). The sequencing data were analyzed by Inference of CRISPR
219 Edits (ICE) v2 CRISPR analysis tool. The sgRNA target sequences and PCR primer
220 sequences are listed in Table S1.

221 **Zebrafish RNA extraction and real-time quantitative PCR (RT-qPCR)**

222 Total RNA at different developmental stages, adult tissues, and CRISPR/Cas9
223 injected larvae were extracted using the TRIzol Reagent (Thermo Fisher Scientific, CA,
224 USA) and purified by RNA clean and concentrator-5 kit (Zymo Research, CA, USA)
225 according to the manufacturer's instructions. RNA concentration was measured by
226 DeNovix DS-11 spectrophotometer (DeNovix Inc. USA). The cDNA was synthesized by
227 iScript RT Supermix (Bio-Rad, USA), and was used as a template for performing the
228 RT-qPCR with SYBR Green Supermix (Thermo Fisher Scientific, CA, USA) and the
229 Light Cycler® 96 System (Roche, CA, USA). All RT-qPCR reactions were carried out
230 using three biological and technical replicates. The housekeeping gene *18S* was used
231 as a reference gene.

232 All RT-qPCR primer pairs were designed across exon-exon junctions using NCBI
233 Primer-BLAST program. The sequences are listed in Table S1. The PCR cycling

234 conditions were used as per the manufacturer instructions, and the amplification
235 specificity was assessed by dissociation curve analysis at the end of the PCR cycles.
236 The cycle threshold values (Ct) data were imported into Microsoft Excel for the relative
237 gene expression analysis. Quantification was based on $2^{(-\Delta\Delta CT)}$ method (Livak and
238 Schmittgen, 2001), and using 18 hours post fertilization (hpf) for *clarin 2* temporal
239 expression, muscle for *clarin 2* in different tissue expression and the corresponding age-
240 matched control for *clarin 2* CRISPR injected F₀ larvae as normalization control.

241 **Distribution of *clrn2* and phalloidin staining in zebrafish**

242 To determine *clrn2* expression, we used in situ hybridization on larvae and inner
243 ear-containing cryosections. The full-length coding sequence of zebrafish *clarin 2*
244 (NM_001114690.1) was PCR amplified from WT zebrafish cDNA using primer pairs with
245 restriction enzymes *Bam*HI and *Xho*I restriction sites cloned into pCS2+ vector (a kind
246 gift from Dr. Dave Turner, University of Michigan). After restriction digestion, the
247 resulting clones were sequenced and used as templates for riboprobe synthesis. The
248 digoxigenin-UTP-labeled riboprobes were synthesized according to the manufacturer's
249 instructions (Millipore Sigma, MO, USA). Briefly, the *clarin 2* and the *pvalb9* plasmids
250 (Horizon Discovery) were linearized by *Bam*HI and *Not*I restriction enzymes,
251 respectively. The linearized plasmid was purified and used as template for in vitro
252 transcription using T7 RNA polymerase to synthesize anti-sense probes. The sense
253 probe was made using *Xba*I linearized *clarin 2* plasmid and SP6 RNA polymerase.

254 The whole-mount in situ hybridization (WISH) on 3 and 5 dpf zebrafish
255 embryos/larvae was performed following the procedures as described by Thisse et al.

256 with minor modifications that can be found in the Supplementary Methods (Thisse and
257 Thisse, 2008).

258 For preparation of cryo-section samples after WISH, the 5 dpf larvae were
259 soaked in 25%, 30% (V/V) sucrose/PBS and optimum cutting temperature (OCT) each
260 for at least two days, and embedded in OCT then Cryotome sectioned at a 10-
261 micrometer thickness.

262 For phalloidin staining of the zebrafish inner ear, 5 dpf larvae were euthanized
263 with tricaine and fixed in 4% (V/V) paraformaldehyde (PFA) at 5 dpf, fixed embryos
264 were washed by PBSTx (1% PBS, 0.2% triton X-100) and incubated in 2% triton X-100
265 in PBS at room temperature for overnight with agitation until the otoliths were
266 completely dissolved. The larvae were sequentially washed in PBSTx and incubated
267 with Alexa Fluor 647 Phalloidin (1:100) (Thermo Fisher Scientific, CA, USA) in PBSTw
268 (1% PBS, 0.1% Tween-20) at room temperature for 4 hours. The samples were washed
269 in PBSTx after staining and mounted laterally in 75% glycerol on slides. Images were
270 acquired with a Zeiss LSM-710 Confocal microscope.

271 **Production and phenotyping of clarin 2 deficient mutant in mice**

272 The *Cln2*^{del629} mutant line was generated on a C57BL/6N background by the
273 Molecular and Cellular Biology group at the Mary Lyon Centre (MLC), MRC Harwell
274 Institute, using CRISPR/Cas9 genome editing (Dunbar et al., 2019). The mice were
275 housed and maintained under specific pathogen-free conditions in individually ventilated
276 cages, with environmental conditions as outlined in the Home Office Code of Practice.
277 Animals were housed with littermates until weaned, and then housed with mice of the
278 same sex and of similar ages, which was often their littermates. Both male and female

279 animals were used for all experiments. Animal procedures at the MRC Harwell Institute
280 were licenced by the Home Office under the Animals (Scientific Procedures) Act 1986,
281 UK and additionally approved by the Institutional Animal Welfare and Ethical Review
282 Body (AWERB). The *Cln1*^{-/-} mice (*Cln1*^{tm1.2Ugpa}, MGI: 6099052) used for comparative
283 scanning electron microscopy analyses were previously described (Dulon et al., 2018).

284 Auditory Brainstem Response (ABR) tests were performed using a click stimulus
285 and frequency-specific tone-burst stimuli (at 8, 16 and 32 kHz) to screen mice for
286 auditory phenotypes and investigate auditory function (Hardisty-Hughes et al., 2010).
287 Distortion Product Oto-Acoustic Emission (DPOAE) tests were performed using
288 frequency-specific tone-burst stimuli from 8 to 32 kHz with the TDT RZ6 System 3
289 hardware and BioSig RZ software (Tucker Davis Technology, Alachua, FL, USA).
290 Detailed descriptions of ABR and DPOAE testing can be found in the Supplementary
291 Methods.

292 Mice were euthanized by cervical dislocation and inner ears were removed and
293 fixed in 2.5% glutaraldehyde (TAAB Laboratories Equipment Ltd.) in 0.1 M phosphate
294 buffer (Sigma-Aldrich) overnight at 4°C. Following decalcification in 4.3% EDTA,
295 cochleae were sub-dissected to expose the sensory epithelium then 'OTO processed'
296 with alternating incubations in 1% osmium tetroxide (TAAB Laboratories Equipment
297 Ltd.) in 0.1 M sodium cacodylate (Sigma-Aldrich) and 1% thiocarbohydrazide (Sigma-
298 Aldrich) in ddH₂O. Ears were dehydrated through a graded ethanol (Fisher Scientific)
299 series (25% to 100%) at 4°C and stored in 100% acetone (VWR Chemicals) until critical
300 point drying with liquid CO₂ using an Emitech K850 (EM Technologies Ltd). Ears were
301 mounted onto stubs using silver paint (Agar Scientific), sputter coated with palladium

302 using a Quorum Q150R S sputter coater (Quorum Technologies) and visualised with a
303 JSM-6010LV Scanning Electron Microscope (JEOL). Micrographs were pseudo-
304 coloured in Adobe Photoshop.

305 **Results**

306 **Identification of *CLRN2* as a novel deafness gene in a consanguineous Iranian** 307 **family exhibiting autosomal recessive non-syndromic sensorineural hearing loss**

308 A three generation Iranian family of Lurs ethnicity was ascertained as part of a
309 large ethnically diverse Iranian population rare disease study (Fig. 1A). Three
310 individuals that included the proband (IV-6), his sibling (IV-1), and a cousin (IV-8), born
311 from consanguineous marriages, have reported moderate-to-profound bilateral non-
312 syndromic sensorineural hearing loss (Fig. 1B). The age of onset for these three
313 individuals was between 2 and 3 years of age. Pure-tone air- and bone-conduction
314 audiometry thresholds (Fig. 1B) show evidence of intrafamilial variability. Individual IV-1
315 has a down sloping audiogram, with bilateral moderate-to-profound deafness. Individual
316 IV-6 presented a moderate-to-severe hearing loss with slightly better hearing at higher
317 frequencies. Both individuals showed normal (type A) tympanograms bilaterally. Speech
318 recognition thresholds for individual IV-1 were 80 dB and 75 dB at 84% and 88% for
319 right and left ears, respectively, and a most comfortable level of 95 dB. Speech
320 recognition thresholds for individual IV-6 were 75 dB and 80 dB, each at 84%, for right
321 and left ears, respectively. Patients have normal neuromotor, speech and language
322 development, and did not show signs of impaired balance. No other abnormalities,
323 including potential vision deficit, were present in the affected individuals, who were last
324 evaluated at the age of 29 (IV-1), 44 (IV-6), and 25 (IV-8) years. For comparison, pure-
325 tone audiometry was also recorded from a family member (V-1), with no reported history
326 of hearing problem.

327 To identify the underlying genetic lesion, we applied homozygosity mapping in
328 the extended family to identify a 15.2 Mb locus on chromosome 4p15.32p15.1
329 (GRCh37/hg19, chr4:17,298,445-32,495,165), defined by the SNPs rs7692897 and
330 rs17081424 (Fig. 1C, Fig. S1A, Table S2). This locus contains 30 genes, none of which
331 are presently associated with deafness in humans (Table S3). This approach also
332 revealed four much smaller homozygous intervals on chromosomes 2p21 (137.3 kb),
333 3p22.2 (262.5 kb), 13q13.1 (90.7 kb), and 17q21.31 (292.6 kb) (Fig. S1A, Table S2) that
334 do not contain known deafness-associated genes (Table S3). Pathogenic copy number
335 variations were excluded. Next, we undertook exome sequencing of affected individual
336 IV-6 (arrow, Fig. 1A). This generated 56,387,543 mappable reads, with 75.5% on-target
337 reads. The mean depth was 57.3-fold, with 97.3% of regions with a 10-fold read depth.
338 Analysis of the exome data of individual IV-6 excluded any candidate pathogenic
339 variants in known deafness-associated genes (Doll et al., 2020) prompting an exome-
340 wide analysis followed by filtering and re-analysis of variants in homozygous intervals
341 (Table S4). Further, close inspection of the exome sequencing data revealed complete
342 sequencing coverage of genes in the homozygous intervals (Table S5). Variant filtering
343 detected a homozygous missense variant in *CLRN2* c.494C>A, (p.(Thr165Lys))
344 (NM_001079827.2) in the 15.2 Mb homozygous interval on chromosome 4 (Fig. S1A,
345 S1B). This variant was shared with individual IV-1 and segregated in the extended
346 family comprising a total of 14 individuals (Fig. 1A, D). Only individuals homozygous for
347 the *CLRN2* c.494C>A variant exhibit hearing loss confirming the recessive nature of the
348 allele (Fig. 1A).

349 **The *CLRN2* c.494C>A leads to a pathogenic missense substitution and aberrant**
350 **splicing**

351 The c.494C>A variant on chromosome 4p15.32 is unanimously predicted to be
352 deleterious and disease causing by *in silico* tools (Table S6). The c.494C>A variant in
353 *CLRN2* replaces a polar uncharged amino acid (threonine) with a positively charged
354 amino acid (lysine) in clarin 2, (p.(Thr165Lys)) (Creixell et al., 2012). This variant, as
355 well as homozygous loss-of-function alleles are absent in population frequency
356 databases. This suggests *CLRN2* is intolerant to biallelic loss-of-function. Our in-house
357 collection of 16,041 additional exomes of simplex patients with predominantly Iranian,
358 Pakistani and Egyptian ethnicities, including 462 exomes of probands with autosomal
359 recessive hearing loss, identified only one hearing impaired individual who carried the
360 c.494C>A variant in *CLRN2* (allele frequency 3.12×10^{-5}). An additional multiethnic
361 cohort (Iranian, European American and Indian) that consists of 380 probands with
362 autosomal recessive hearing loss ranging from moderate-to-profound was also
363 screened for variants in *CLRN2*, but none were identified.

364 The c.494C>A variant involves the exchange of a novel polar threonine (Thr)
365 residue to a basic lysine (Lys) amino acid that affects a highly conserved amino acid in
366 the alpha-helix of the PMP-22/EMP/MP20/Claudin superfamily domain (Fig. 2A-C).
367 Among clarin proteins, clarin 2 and clarin 1 show 34.9% identity with 81 identical and 91
368 similar amino acids (using UniProt (UniProt Consortium, 2018), Fig. 2B). The outcome
369 of *CLRN1* pathogenic or likely pathogenic missense variants, as well as nonsense
370 variants (queried from the Deafness Variation Database v8.2 (Azaiez et al., 2018)) are
371 marked in red (Fig. 2B) along with the clarin 2 p.(Thr165Lys) amino acid substitution

372 (Fig. 2B, asterisk). Interestingly, nine out of the 19 clarin 1 amino acid mutated residues
373 are identical in clarin 2. Three clarin 1 amino acid substitutions (p.(Leu163Pro),
374 p.(Leu167Trp), and p.(Ile181Asn), NP_001182723.1) align in close proximity to the
375 clarin 2 p.(Thr165Lys). Furthermore, clarin 1 p.Leu163Pro (Fields et al., 2002) and
376 p.Ile181Asn (García-García et al., 2012), that are both reported in USH3A, are
377 p.Leu150 and p.Ile168 in clarin 2. Most importantly, the threonine residue at position
378 165 (Thr165) CLRN2 is conserved across species and the corresponding amino acid in
379 clarin 1 is a serine residue (Fig. 2A,B), a scenario often associated with conserved
380 phosphorylation site residue, here by serine/threonine protein kinases (Creixell et al.,
381 2012).

382 In addition to causing an amino acid missense substitution, computational
383 analysis also predicts that the c.494C>A variant will create an exonic splicing enhancer
384 (ESE) motif, modifying the ESE hexameric sequence landscape of exon 3, which could
385 interfere with the normal processing of *CLRN2* mRNA (Figs. S2A, S3B; ESEfinder and
386 RESCUE-ESE, Human Splicing Finder) (Cartegni et al., 2003; Desmet et al., 2009;
387 Fairbrother et al., 2004). To investigate the effect of the c.494C>A variant on *CLRN2*
388 splicing, we used mini-gene assays using two different exon-trapping vectors and three
389 different cell lines, Cos-7, ARPE-19, and HEK 293T. The mini-gene contained the 3'
390 end of intron 2, all of exon 3 (with and without the *CLRN2* variant), and ~50 bp of the 3'
391 UTR (Fig. 3A) and was transfected into COS-7 and ARPE-19 cells. As a negative
392 *CLRN2* control, we used the rs117875715 SNP, a common polymorphism, with a global
393 minor allele frequency of ~1.25% and >100 homozygous alleles reported in gnomAD
394 (Lek et al., 2016) (<http://gnomad.broadinstitute.org/variant/4-17528480-G-A>) that is 20

395 nucleotides away from c.494C>A. Given its frequency, rs117875715 is predicted to be
396 benign for hearing loss. Of note, this polymorphism is absent in the proband and family
397 members reported here. Since exon 3 is the last exon of *CLRN2*, we designed our PCR
398 primers to exclude the human poly-A signal and used the poly-A signal native to the
399 pET01 vector. As expected for WT *CLRN2* (c.494C), we detected the splicing of the 5'
400 native pET01 exon only to exon 3 of *CLRN2* (Fig. 3A, B). The same normal splicing was
401 obtained in all cell types transfected with *CLRN2* containing the control (rs117875715)
402 variant (Fig. 3B). However, the c.494C>A variant yielded two bands; one ~650 bp band
403 matching the expected normally spliced exon, and a second abnormal band that was
404 approximately ~1,360 bp (Fig. 3B). Sequencing of these amplicons validated normal
405 splicing including the c.494A variant and also revealed a retained intron 2 in the
406 aberrantly spliced transcript (Fig. S3C). The retention of intron 2 results in a new
407 reading frame that introduces a stop codon 26 amino acids after the native exon 2
408 splice site (p.(Gly146Lysfs*26)) (Fig. 3C). These results were replicated using the
409 pSPL3b vector and HEK 293T cells (Fig. S3A-C), confirming the c.494C>A induced
410 normal and aberrant splicing, independent of the cell type context. Following TA-cloning
411 of cDNA amplicons from the homozygous individual (from Fig. S3B), 23 of 26 amplicons
412 (88.5%) showed normal splicing, and 3 of 26 amplicons (11.5%) showed a retained
413 intron.

414 The mini-gene splicing assays and sequence analyses clearly show that the
415 c.494C>A affects a highly conserved and key residue in clarin 2 sequence, while also
416 creating aberrant mRNA splicing *in vivo* likely leading to a truncated protein. Altogether,
417 this further confirms that variants in *CLRN2* can lead to sensorineural hearing loss.

418 ***Clnr2*, a hair cell expressed gene key to hearing also in zebrafish and mice**

419 To further study the role of clarin 2 in the inner ear, we investigated its
420 expression and analyzed potential impact of *Clnr2* loss-of-function in two other species,
421 zebrafish and mice.

422 ***clnr2* in zebrafish**

423 Taking advantage of larva transparency, we used zebrafish as a model to
424 investigate the *clarin 2* expression during early embryonic development. The RT-qPCR
425 at different developmental stages revealed that *clnr2* mRNA was first detected at 18 hpf
426 (Fig. 4A), a stage when the otic placode begins to form the otic vesicle in zebrafish (this
427 stage is similar to mouse embryonic day 9 (E9), a stage of otic placode formation)
428 (Kopecky et al., 2012; Whitfield et al., 2002). *clnr2* mRNA expression increased (2-fold
429 at 72 and 96 hpf compared to 18 hpf) and was maintained at later stages, up to 120 hpf
430 (Fig. 4A). Comparative analyses of *clnr2* mRNA expression in different adult tissues of
431 zebrafish revealed a significant enrichment in utricle, saccule and lagena of the inner
432 ear (Fig. 4B). Our data are in agreement with RNA expression data from the Genotype-
433 Tissue Expression (GTEx) project, wherein *CLRN2* mRNA in humans is enriched in the
434 nervous system, testis, kidney, salivary gland, and lung. *CLRN1* has a similar
435 expression profile in humans.

436 To determine *clnr2* cellular expression, we used WISH in the inner ear of 3- and
437 5-dpf embryos (Fig. 4C, D). Unlike the *clnr2* sense probe, the anti-sense *clnr2* revealed
438 strong expression in the otic vesicle, similar to the expression of anti-sense *pvalb9*,
439 used as a marker of hair cells (Fig. 4C). Histological examination of 5 dpf embryos

440 further confirmed that *clrn2* expression is more specifically, restricted to hair cells, and is
441 not expressed in the supporting cells of the inner ear (Fig. 4D).

442 To elucidate the function of *clrn2* in zebrafish, we used CRISPR/Cas9 to
443 generate loss-of-function alleles. To maximize the knockout efficiency, we used five
444 sgRNAs targeting the first and second exon of *clrn2* gene (Fig. S4). Injected embryos
445 (crispants) were sequenced and, as expected, a mix of alleles in the form of deletions
446 ranging from 4 bp to 73 bp, as well as insertions spanning +1 to +11 bp were observed.
447 The majority of the variants were frameshift that would most likely create a premature
448 stop codon in the protein (Fig. S4). The RT-qPCR analyses on injected embryos
449 showed that *clrn2* crispants have a significantly reduced amount of *clrn2* mRNA (Fig.
450 4E), suggesting nonsense mediated decay, leading to disrupted clarin 2 protein
451 function.

452 Considering the expression in hair cells (Fig. 4D), we investigated the
453 mechanosensory structures of the hair cell bundle, which are important for hearing and
454 balance function in zebrafish. Interestingly, fluorescent phalloidin staining of the hair
455 bundles of the inner ear in *clrn2* crispants (n=10) showed disrupted hair bundle structure
456 compared to the WT controls; the hair bundles are splayed, thin and split in *clrn2*
457 crispants (arrowheads in Fig. 4E). This defective phenotype, suggesting a critical role in
458 hair bundle structures, is similar to the hair bundles in zebrafish *clrn1* knockouts (Gopal
459 et al., 2015), the *orbiter* mutants (defective in *protocadherin 15 (pcdh15)*, a gene
460 associated with human Usher syndrome 1F) (Seiler et al., 2005) and *ush1c* morphants
461 and *ush1c* mutants (Phillips et al., 2011).

462 ***Clrn2* in mice**

463 To further assess the requirement of clarin 2 for auditory function in mammals,
464 and assess further its role in auditory hair bundles, we extended our analyses to mouse.
465 Consistent with expression data in zebrafish (Fig. 4A, C, D), single cell RNA-seq data
466 available to visualize on the gEAR portal (umgear.org) show that in the mouse cochlear
467 epithelium at postnatal day 1 (P1) and P7, *Cln2* transcripts are almost exclusively
468 detectable only in inner and outer hair cell populations (Kolla et al., 2020) (see also Fig.
469 S5). We utilized a CRISPR/Cas9-engineered *Cln2* loss-of-function mouse mutant, in
470 which exon 2 has been deleted (*Cln2*^{del629}) (Fig. 5A), and measured ABRs in P21 (\pm 1
471 day) mice in response to click and tone-burst stimuli.

472 Analysis of ABR thresholds, which is the lowest sound stimulus required to elicit
473 measurable activity in the auditory nerve, showed that homozygous (*Cln2*^{del629/del629})
474 mice display very elevated thresholds (>80 decibel sound pressure level (dB SPL)) at all
475 frequencies tested: 8, 16 and 32 kHz (Fig. 5B). Whereas, *Cln2*^{del629/+} mice exhibit
476 thresholds comparable with those of WT (*Cln2*^{+/+}) littermates (<40 dB SPL),
477 demonstrating the absence of a heterozygous auditory phenotype (Fig. 5B).

478 To further assess cochlear function, DPOAEs were measured in P28 (\pm 1 day)
479 *Cln2*^{del629/del629} mice. Compared to their *Cln2*^{+/+} and *Cln2*^{del629/+} littermates,
480 *Cln2*^{del629/del629} mice have reduced DPOAEs (Fig. 5B) suggesting impaired outer hair
481 cell (OHC) function.

482 To investigate stereocilia bundle morphology in *Cln2*^{del629/del629} mice, we used
483 scanning electron microscopy to examine the cochlear sensory epithelia. At P28 (\pm 1
484 day), the inner and outer hair cell stereocilia bundles of *Cln2* mutant mice display the
485 expected U- and V- shape, respectively, which contrasts with the grossly misshapen

486 OHC bundles found in *Cln1* mutant mice (Fig. 5C). However, while the patterning of the
487 bundles appears normal in *Cln2*^{del629/del629} mice the heights of their middle and short
488 row stereocilia are visibly more variable compared with those of *Cln2*^{+/+} littermates, and
489 many of the short row 'mechanotransducing' stereocilia are missing (Fig. 5C).

490 Together, our findings establish that clarin 2 is key to hearing function in
491 zebrafish and mouse, and likely has a key role in the mechanotransducing stereocilia of
492 the hair bundle.

493

494 Discussion

495 We identify *CLRN2* as a novel deafness gene in human and zebrafish and
496 describe a new deafness-causing allele in mice. Genetic study using homozygosity
497 mapping and exome sequencing of an extended Iranian family with multiple
498 consanguineous marriages identified a pathogenic variant, c.494C>A in exon 2 of
499 *CLRN2* segregating with pre-lingual ARNSHL. The c.494C>A variant results in a
500 missense and splicing defect in clarin 2. By producing mutant zebrafish and mice
501 lacking clarin 2, we demonstrated the key role the protein plays to ensure normal
502 structural and functional integrity of the hair bundle, the sound- and motion- receptive
503 structure of inner ear hair cells.

504 The clarin gene family also includes the *CLRN1* gene. Pathogenic variants in
505 *CLRN1* have been linked to variable clinical outcomes, ranging from non-syndromic RP
506 (Khan et al., 2011) to USH3A characterized by variable and progressive post-lingual
507 hearing loss, RP, and variable vestibular responses (Plantinga et al., 2005). Several

508 cases of later onset HL and/or RP, as late as the sixth decade of life, have been
509 reported for USH3A patients (Ness et al., 2003). Clinical examination of affected
510 individuals in this family, at the age of 25 (IV-8), 29 (IV-1), and 44 (IV-6) years of age,
511 excluded the presence of additional syndromic features showing that homozygosity for
512 the c.494C>A variant causes non-syndromic hearing loss, ranging from moderate-
513 severe (IV-6) to profound (IV-1) deafness (Fig. 1A, B).

514 The c.494C>A variant affects an amino acid that is highly conserved among
515 PMP-22/EMP/EP20/Claudin superfamily proteins (Fig. 2A-C). In addition, the c.494
516 cytosine is highly conserved and the exchange to adenine is predicted to create an ESE
517 site that likely impacts splicing efficiency in humans (Fig. S2A, B) but not zebrafish (Fig.
518 S2C). We confirmed the effect on splicing using mini-gene assays. We showed that the
519 c.494C>A variant acts in two ways: 1) as a missense variant (p.Thr165Lys) producing a
520 mutant full length protein and 2) as a splice variant leading to intron retention (Fig. 3B,
521 and Fig. S3B, C) expected to cause a premature stop codon 26 amino acids into intron
522 2 (p.Gly146Lysfs*26) (Fig. 3C).

523 Variants that disrupt splicing machinery signals can impact accurate recognition
524 and removal of intronic sequences from pre-mRNA (Fairbrother et al., 2004) and are
525 recognized as significant contributors to human genetic diseases (Xiong et al., 2015).
526 ESE sequences are *cis*-acting elements primarily recognized by the SR family proteins
527 that function by recruiting core splicing machinery components to splice sites or by
528 acting antagonistically against nearby silencing elements (Fairbrother et al., 2004;
529 Graveley, 2000; Kan and Green, 1999). ESEs are often associated with introns that

530 contain weak splicing signals, but they can also reside in exons and impact the splicing
531 process.

532 Two potential mechanisms could synergistically contribute to the disruptive effect
533 of the missense variant. *First*, the replacement of threonine with lysine, an amino acid
534 with a positively charged 'bulky' side chain (lysine), may affect protein folding (Creixell et
535 al., 2012) and transport to the plasma membrane. Membrane proteins sort to the
536 plasma membrane via the conventional secretory pathway associated with ER-to-Golgi
537 complex (Viotti, 2016). Misfolded membrane proteins are typically retained in the
538 endoplasmic reticulum (ER) and degraded by the ER-associated degradation pathway
539 (Kincaid and Cooper, 2007; Sano and Reed, 2013). It is possible that a small fraction of
540 the misfolded clarin 2 p.(Thr165Lys) could reach the plasma membrane via the
541 unconventional secretory pathway, similar to that reported for clarin 1 p.(Asn48Lys)
542 (p.(N48K)) (Gopal et al., 2019). The unconventional secretory pathway is induced by the
543 ER-associated misfolded or unfolded protein response (Kinseth et al., 2007; Schröder
544 and Kaufman, 2005). However, the mutant clarin 2 reaching the surface may be
545 functionally inactive. *Second*, evolutionarily conserved threonine residues are also
546 conserved protein phosphorylation sites. Phosphorylation adds a negative charge to the
547 side chain of the amino acid and it serves as an important post-translational mechanism
548 for regulation of protein function (Pearlman et al., 2011). Loss of threonine at position
549 165 would potentially prevent functional activation of clarin 2. However, additional
550 experiments are essential to test these hypotheses and unravel the true pathogenic
551 mechanism associated with the p.(Thr165Lys) missense variant.

552 Our *in situ* hybridization in zebrafish (Fig. 4C, D) and *in silico* analyses (Fig. S5)
553 in mouse clearly support predominant expression of *Clrn2* in the sensory hair cells. To
554 examine further the key role of clarin 2 in the inner ear, we generated zebrafish and
555 mice lacking a functional protein. ABR measurements in *Clrn2*^{del629/del629} mice revealed
556 an early-onset hearing loss with elevated hearing thresholds compared with their
557 *Clrn2*^{+/+} littermate controls (mean click threshold 87 dB SPL ± 7 s.d. and 24 dB SPL ± 6
558 s.d., respectively). These data are consistent with early-onset hearing loss observed in
559 another loss-of-function *Clrn2* mutant (*Clrn2*^{clarinet}), which harbors an early truncating
560 nonsense variant (p.Trp4*) (Dunbar et al., 2019). Interestingly, unlike observations in
561 humans with *CLRN1* pathogenic variants, neither *Clrn1* (Dulon et al., 2018; Geller et al.,
562 2009; Geng et al., 2009) nor *Clrn2* (Dunbar et al., 2019) knockout mice exhibit a retinal
563 phenotype. In the inner ear, the reduced DPOAEs in both *Clrn2*^{del629/del629} and in
564 *Clrn2*^{clarinet/clarinet} mice (Dunbar et al., 2019), indicates impairment of OHCs function. This,
565 together with the severe-to-profound hearing loss already exhibited at P21 in *Clrn2*
566 mutant mice points to gene defects likely affecting both inner hair cells (IHCs) and
567 OHCs. This is further supported by scanning electron microscopy data showing loss of
568 shortest row stereocilia in both the cochlear IHCs and OHCs (Fig. 5C). Phalloidin
569 staining of *clrn2* crispants also confirms hair bundle abnormalities in zebrafish.

570 In regard to the observed progressivity of the hearing impairment in *clarinet* mice
571 (Dunbar et al., 2019), the earliest reported clinical diagnosis of hearing loss of the
572 *CLRN2* affected individuals in the family we present is between 2 and 3 years of age.
573 Newborn hearing screening was not routinely performed when the affected individuals
574 were born, so we cannot confirm hearing was normal at birth. In light of absent serial

575 audiograms, we cannot report if the hearing loss experienced in these patients is
576 progressive, as is observed in the mouse model (Dunbar et al., 2019).

577 In conclusion, we demonstrate the c.494C>A variant affects exon 3 splicing
578 efficiency. We showed, for the first time, that *CLRN2* is a deafness-causing gene in
579 humans. A variant causes hearing loss in humans, replicated by animal studies.
580 Additional reports of families segregating *CLRN2* biallelic variants will be crucial to
581 refine and dissect the clinical course and characteristics of hearing loss due to this
582 gene. Together, our studies in zebrafish and mice establish that hearing loss is probably
583 due to defective protein in the hair cells, where the presence of clarin 2 is essential for
584 normal organization and maintenance of the mechanosensitive hair bundles.

585 **Acknowledgements**

586 We would like to extend our gratitude to the family for their participation. We thank Dr.
587 Caroline Lekszas, Dr. Daniel Liedtke, and Dr. Indrajit Nanda from the Institute of Human
588 Genetics at the University of Würzburg for their technical expertise. This work was
589 supported by Intramural Funding (fortune) at the University of Tübingen (2545-1-0 to
590 B.V.), the Ministry of Science, Research and Art Baden-Württemberg (to B.V.), the
591 Medical Research Council (MC_UP_1503/2 to M.R.B), ANR light4deaf (ANR-15-RHUS-
592 0001), HearInNoise (ANR-17-CE16-0017), LHW-stiftung to A.E.), and a grant from
593 NIH/COBRE GM103636 (Project 3); the Presbyterian Health Foundation (PHF) Grant to
594 GKV. This study was funded in part by NIDCDs R01s DC002842 and DC012049 to RJS
595 and T32 GM007748 to KTB. LAD is a Medical Research Council DPhil student
596 (1774724).

597 **References**

- 598 Adato, A., S. Vreugde, T. Joensuu, N. Avidan, R. Hamalainen, O. Belenkiy, T. Olender,
599 B. Bonne-Tamir, E. Ben-Asher, C. Espinos, J.M. Millán, A.E. Lehesjoki, J.G. Flannery,
600 K.B. Avraham, S. Pietrokovski, E.M. Sankila, J.S. Beckmann, and D. Lancet. 2002.
601 USH3A transcripts encode clarin-1, a four-transmembrane-domain protein with a
602 possible role in sensory synapses. *Eur J Hum Genet* 10:339-350.
- 603 Adzhubei, I.A., S. Schmidt, L. Peshkin, V.E. Ramensky, A. Gerasimova, P. Bork, A.S.
604 Kondrashov, and S.R. Sunyaev. 2010. A method and server for predicting damaging
605 missense mutations. *Nat Methods* 7:248-249.
- 606 Azaiez, H., K.T. Booth, S.S. Ephraim, B. Crone, E.A. Black-Ziegelbein, R.J. Marini, A.E.
607 Shearer, C.M. Sloan-Heggen, D. Kolbe, T. Casavant, M.J. Schnieders, C. Nishimura, T.
608 Braun, and R.J.H. Smith. 2018. Genomic Landscape and Mutational Signatures of
609 Deafness-Associated Genes. *Am J Hum Genet* 103:484-497.
- 610 Booth, K.T., H. Azaiez, K. Kahrizi, D. Wang, Y. Zhang, K. Frees, C. Nishimura, H.
611 Najmabadi, and R.J. Smith. 2018a. Exonic mutations and exon skipping: Lessons
612 learned from DFNA5. *Hum Mutat* 39:433-440.
- 613 Booth, K.T., K. Kahrizi, H. Najmabadi, H. Azaiez, and R.J. Smith. 2018b. Old gene, new
614 phenotype: splice-altering variants in CEACAM16 cause recessive non-syndromic
615 hearing impairment. *J Med Genet* 55:555-560.
- 616 Cartegni, L., J. Wang, Z. Zhu, M.Q. Zhang, and A.R. Krainer. 2003. ESEfinder: A web
617 resource to identify exonic splicing enhancers. *Nucleic Acids Res* 31:3568-3571.

618 Chun, S., and J.C. Fay. 2009. Identification of deleterious mutations within three human
619 genomes. *Genome Res* 19:1553-1561.

620 Creixell, P., E.M. Schoof, C.S. Tan, and R. Linding. 2012. Mutational properties of
621 amino acid residues: implications for evolvability of phosphorylatable residues. *Philos*
622 *Trans R Soc Lond B Biol Sci* 367:2584-2593.

623 Cunningham, C.L., and U. Müller. 2019. Molecular Structure of the Hair Cell
624 Mechanoelectrical Transduction Complex. *Cold Spring Harb Perspect Med* 9:pii:
625 a033167.

626 Desmet, F.O., D. Hamroun, M. Lalande, G. Collod-Beroud, M. Claustres, and C.
627 Beroud. 2009. Human Splicing Finder: an online bioinformatics tool to predict splicing
628 signals. *Nucleic Acids Res* 37:e67.

629 Doll, J., M.A.H. Hofrichter, P. Bahena, A. Heihoff, D. Segebarth, T. Müller, M. Dittrich, T.
630 Haaf, and B. Vona. 2020. A novel missense variant in MYO3A is associated with
631 autosomal dominant high-frequency hearing loss in a German family. *Mol Genet*
632 *Genomic Med* e1343.

633 Dulon, D., S. Papal, P. Patni, M. Cortese, P.F. Vincent, M. Tertrais, A. Emptoz, A. Tlili,
634 Y. Bouleau, V. Michel, S. Delmaghani, A. Aghaie, E. Pepermans, O. Alegria-Prevot, O.
635 Akil, L. Lustig, P. Avan, S. Safieddine, C. Petit, and A. El-Amraoui. 2018. Clarin-1 gene
636 transfer rescues auditory synaptopathy in model of Usher syndrome. *J Clin Invest*
637 128:3382-3401.

638 Dunbar, L.A., P. Patni, C. Aguilar, P. Mburu, L. Corns, H.R. Wells, S. Delmaghani, A.
639 Parker, S. Johnson, D. Williams, C.T. Esapa, M.M. Simon, L. Chessum, S. Newton, J.
640 Dorning, P. Jeyarajan, S. Morse, A. Lelli, G.F. Codner, T. Peineau, S.R. Gopal, K.N.
641 Alagramam, R. Hertzano, D. Dulon, S. Wells, F.M. Williams, C. Petit, S.J. Dawson, S.D.
642 Brown, W.A.-O. Marcotti, A.A.-O. El-Amraoui, and M.A.-O.X. Bowl. 2019. Clarin-2 is
643 essential for hearing by maintaining stereocilia integrity and function. *EMBO Mol Med*
644 11:e10288.

645 Fairbrother, W.G., G.W. Yeo, R. Yeh, P. Goldstein, M. Mawson, P.A. Sharp, and C.B.
646 Burge. 2004. RESCUE-ESE identifies candidate exonic splicing enhancers in vertebrate
647 exons. *Nucleic Acids Res* 32:W187-190.

648 Fattahi, Z., M. Beheshtian, M. Mohseni, H. Poustchi, E. Sellars, H. Nezhadi, A. Amini, S.
649 Arzhang, K. Jalalvand, P. Jamali, Z. Mohammadi, B. Davarnia, P. Nikuei, M. Oladnabi,
650 A. Mohammadzadeh, E. Zohrehvand, A. Nejatizadeh, M. Shekari, M. Bagherzadeh, E.
651 Shamsi-Gooshki, S. Borno, B. Timmermann, A. Haghdoost, R. Najafipour, H.R.K.
652 Khorshid, K. Kahrizi, R. Malekzadeh, M.R. Akbari, and H. Najmabadi. 2019. Iranome: A
653 catalogue of genomic variations in the Iranian population. *Hum Mutat*

654 Fields, R.R., G. Zhou, D. Huang, J.R. Davis, C. Möller, S.G. Jacobson, W.J. Kimberling,
655 and J. Sumegi. 2002. Usher syndrome type III: revised genomic structure of the USH3
656 gene and identification of novel mutations. *Am J Hum Genet* 71:607-617.

657 García-García, G., M.J. Aparisi, R. Rodrigo, M.D. Sequedo, C. Espinós, J. Rosell, J.L.
658 Olea, M.P. Mendivil, M.A. Ramos-Arroyo, C. Ayuso, T. Jaijo, E. Aller, and J.M. Millán.

659 2012. Two novel disease-causing mutations in the CLRN1 gene in patients with Usher
660 syndrome type 3. *Mol Vis* 18:3070-3078.

661 Geller, S.F., K.I. Guerin, M. Visel, A. Pham, E.S. Lee, A.A. Dror, K.B. Avraham, T.
662 Hayashi, C.A. Ray, T.A. Reh, O. Bermingham-McDonogh, W.J. Triffo, S.W. Bao, J.
663 Isosomppi, H. Västinsalo, E.M. Sankila, and J.G. Flannery. 2009. CLRN1 Is
664 Nonessential in the Mouse Retina but Is Required for Cochlear Hair Cell Development.
665 *Plos Genet* 5:

666 Geng, R.S., S.F. Geller, T. Hayashi, C.A. Ray, T.A. Reh, O. Bermingham-McDonogh,
667 S.M. Jones, C.G. Wright, S. Melki, Y. Imanishi, K. Palczewski, K.N. Alagramam, and
668 J.G. Flannery. 2009. Usher syndrome IIIA gene clarin-1 is essential for hair cell function
669 and associated neural activation dagger. *Hum Mol Genet* 18:2748-2760.

670 Gillespie, P.G., and U. Müller. 2009. Mechanotransduction by hair cells: models,
671 molecules, and mechanisms. *Cell* 139:33-44.

672 Gopal, S.R., D.H.C. Chen, S.W. Chou, J.J. Zang, S.C.F. Neuhauss, R. Stepanyan, B.M.
673 McDermott, and K.N. Alagramam. 2015. Zebrafish Models for the Mechanosensory Hair
674 Cell Dysfunction in Usher Syndrome 3 Reveal That Clarin-1 Is an Essential Hair Bundle
675 Protein. *J Neurosci* 35:10188-10201.

676 Gopal, S.R., Y.T. Lee, R. Stepanyan, B.M. McDermott, Jr., and K.N. Alagramam. 2019.
677 Unconventional secretory pathway activation restores hair cell mechanotransduction in
678 an USH3A model. *Proc Natl Acad Sci U S A* 116:11000-11009.

- 679 Graveley, B.R. 2000. Sorting out the complexity of SR protein functions. *RNA* 6:1197-
680 1211.
- 681 Hardisty-Hughes, R.E., A. Parker, and S.D. Brown. 2010. A hearing and vestibular
682 phenotyping pipeline to identify mouse mutants with hearing impairment. *Nat Protoc*
683 5:177-190.
- 684 Hofrichter, M.A.H., M. Mojarad, J. Doll, C. Grimm, A. Eslahi, N.S. Hosseini, M. Rajati, T.
685 Muller, M. Dittrich, R. Maroofian, T. Haaf, and B. Vona. 2018. The conserved p.Arg108
686 residue in S1PR2 (DFNB68) is fundamental for proper hearing: evidence from a
687 consanguineous Iranian family. *Bmc Med Genet* 19:81.
- 688 Hudspeth, A.J. 1997. How hearing happens. *Neuron* 19:947-950.
- 689 Ingham, N.J., S.A. Pearson, V.E. Vancollie, V. Rook, M.A. Lewis, J. Chen, A. Buniello,
690 E. Martelletti, L. Preite, C.C. Lam, F.D. Weiss, Z. Powis, P. Suwannarat, C.J. Lelliott,
691 S.J. Dawson, J.K. White, and K.P. Steel. 2019. Mouse screen reveals multiple new
692 genes underlying mouse and human hearing loss. *PLoS Biol* 17:e3000194.
- 693 Joensuu, T., R. Hamalainen, B. Yuan, C. Johnson, S. Tegelberg, P. Gasparini, L.
694 Zelante, U. Pirvola, L. Pakarinen, A.E. Lehesjoki, A. de la Chapelle, and E.M. Sankila.
695 2001. Mutations in a novel gene with transmembrane domains underlie Usher
696 syndrome type 3. *Am J Hum Genet* 69:673-684.
- 697 Kan, J.L.C., and M.R. Green. 1999. Pre-mRNA splicing of IgM exons M1 and M2 is
698 directed by a juxtaposed splicing enhancer and inhibitor. *Gene Dev* 13:462-471.

699 Kazmierczak, P., H. Sakaguchi, J. Tokita, E.M. Wilson-Kubalek, R.A. Milligan, U. Muller,
700 and B. Kachar. 2007. Cadherin 23 and protocadherin 15 interact to form tip-link
701 filaments in sensory hair cells. *Nature* 449:87-91.

702 Khan, M.I., F.F. Kersten, M. Azam, R.W. Collin, A. Hussain, S.T. Shah, J.E. Keunen, H.
703 Kremer, F.P. Cremers, R. Qamar, and A.I. den Hollander. 2011. CLRN1 mutations
704 cause nonsyndromic retinitis pigmentosa. *Ophthalmology* 118:1444-1448.

705 Kimmel, C.B., W.W. Ballard, S.R. Kimmel, B. Ullmann, and T.F. Schilling. 1995. Stages
706 of embryonic development of the zebrafish. *Dev Dyn* 203:253-310.

707 Kincaid, M.M., and A.A. Cooper. 2007. Misfolded proteins traffic from the endoplasmic
708 reticulum (ER) due to ER export signals. *Mol Biol Cell* 18:455-463.

709 Kinseth, M.A., C. Anjard, D. Fuller, G. Guizzunti, W.F. Loomis, and V. Malhotra. 2007.
710 The golgi-associated protein GRASP is required for unconventional protein secretion
711 during development. *Cell* 130:524-534.

712 Kircher, M., D.M. Witten, P. Jain, B.J. O'Roak, G.M. Cooper, and J. Shendure. 2014. A
713 general framework for estimating the relative pathogenicity of human genetic variants.
714 *Nat Genet* 46:310-315.

715 Kolla, L., M.C. Kelly, Z.F. Mann, A. Anaya-Rocha, K. Ellis, A. Lemons, A.T. Palermo,
716 K.S. So, J.C. Mays, J. Orvis, J.C. Burns, R. Hertzano, E.C. Driver, and M.W. Kelley.
717 2020. Characterization of the development of the mouse cochlear epithelium at the
718 single cell level. *Nat Commun* 11:

719 Kopecky, B., S. Johnson, H. Schmitz, P. Santi, and B. Fritsch. 2012. Scanning thin-
720 sheet laser imaging microscopy elucidates details on mouse ear development. *Dev Dyn*
721 241:465-480.

722 LaFave, M.C., G.K. Varshney, M. Vemulapalli, J.C. Mullikin, and S.M. Burgess. 2014. A
723 defined zebrafish line for high-throughput genetics and genomics: NHGRI-1. *Genetics*
724 198:167-170.

725 Lek, M., K.J. Karczewski, E.V. Minikel, K.E. Samocha, E. Banks, T. Fennell, A.H.
726 O'Donnell-Luria, J.S. Ware, A.J. Hill, B.B. Cummings, T. Tukiainen, D.P. Birnbaum, J.A.
727 Kosmicki, L.E. Duncan, K. Estrada, F. Zhao, J. Zou, E. Pierce-Hoffman, J. Berghout,
728 D.N. Cooper, N. Deflaux, M. DePristo, R. Do, J. Flannick, M. Fromer, L. Gauthier, J.
729 Goldstein, N. Gupta, D. Howrigan, A. Kiezun, M.I. Kurki, A.L. Moonshine, P. Natarajan,
730 L. Orozco, G.M. Peloso, R. Poplin, M.A. Rivas, V. Ruano-Rubio, S.A. Rose, D.M.
731 Ruderfer, K. Shakir, P.D. Stenson, C. Stevens, B.P. Thomas, G. Tiao, M.T. Tusie-Luna,
732 B. Weisburd, H.H. Won, D. Yu, D.M. Altshuler, D. Ardissino, M. Boehnke, J. Danesh, S.
733 Donnelly, R. Elosua, J.C. Florez, S.B. Gabriel, G. Getz, S.J. Glatt, C.M. Hultman, S.
734 Kathiresan, M. Laakso, S. McCarroll, M.I. McCarthy, D. McGovern, R. McPherson, B.M.
735 Neale, A. Palotie, S.M. Purcell, D. Saleheen, J.M. Scharf, P. Sklar, P.F. Sullivan, J.
736 Tuomilehto, M.T. Tsuang, H.C. Watkins, J.G. Wilson, M.J. Daly, D.G. MacArthur, and C.
737 Exome Aggregation. 2016. Analysis of protein-coding genetic variation in 60,706
738 humans. *Nature* 536:285-291.

- 739 Lekszas, C., O. Foresti, I. Raote, D. Liedtke, E.M. König, I. Nanda, B. Vona, P. De
740 Coster, R. Cauwels, V. Malhotra, and T. Haaf. 2020. Biallelic TANGO1 mutations cause
741 a novel syndromal disease due to hampered cellular collagen secretion. *Elife* 9:e51319.
- 742 Livak, K.J., and T.D. Schmittgen. 2001. Analysis of relative gene expression data using
743 real-time quantitative PCR and the 2(T)(-Delta Delta C) method. *Methods* 25:402-408.
- 744 Mazzoli, M., G. Van Camp, V. Newton, N. Giarbini, F. Declau, and A. Parving. 2003.
745 Recommendations for the description of genetic and audiological data for families with
746 nonsyndromic hereditary hearing impairment. *Audiol Med* 1:148-150.
- 747 Morton, C.C., and W.E. Nance. 2006. Newborn hearing screening--a silent revolution. *N*
748 *Engl J Med* 354:2151-2164.
- 749 Ness, S.L., T. Ben-Yosef, A. Bar-Lev, A.C. Madeo, C.C. Brewer, K.B. Avraham, R.
750 Kornreich, R.J. Desnick, J.P. Willner, T.B. Friedman, and A.J. Griffith. 2003. Genetic
751 homogeneity and phenotypic variability among Ashkenazi Jews with Usher syndrome
752 type III. *J Med Genet* 40:767-772.
- 753 Ng, P.C., and S. Henikoff. 2001. Predicting deleterious amino acid substitutions.
754 *Genome Res* 11:863-874.
- 755 Pearlman, S.M., Z. Serber, and J.E. Ferrell, Jr. 2011. A mechanism for the evolution of
756 phosphorylation sites. *Cell* 147:934-946.
- 757 Phillips, J.B., B. Blanco-Sanchez, J.J. Lentz, A. Tallafuss, K. Khanobdee, S. Sampath,
758 Z.G. Jacobs, P.F. Han, M. Mishra, T.A. Titus, D.S. Williams, B.J. Keats, P.

- 759 Washbourne, and M. Westerfield. 2011. Harmonin (Ush1c) is required in zebrafish
760 Müller glial cells for photoreceptor synaptic development and function. *Dis Model Mech*
761 4:786-800.
- 762 Plantinga, R.F., L. Kleemola, P.L. Huygen, T. Joensuu, E.M. Sankila, R.J. Pennings,
763 and C.W. Cremers. 2005. Serial audiometry and speech recognition findings in Finnish
764 Usher syndrome type III patients. *Audiol Neurootol* 10:79-89.
- 765 Sano, R., and J.C. Reed. 2013. ER stress-induced cell death mechanisms. *Biochim*
766 *Biophys Acta* 1833:3460-3470.
- 767 Schröder, M., and R.J. Kaufman. 2005. The mammalian unfolded protein response.
768 *Annu Rev Biochem* 74:739-789.
- 769 Schwarz, J.M., D.N. Cooper, M. Schuelke, and D. Seelow. 2014. MutationTaster2:
770 mutation prediction for the deep-sequencing age. *Nat Methods* 11:361-362.
- 771 Scott, E.M., A. Halees, Y. Itan, E.G. Spencer, Y. He, M.A. Azab, S.B. Gabriel, A.
772 Belkadi, B. Boisson, L. Abel, A.G. Clark, C. Greater Middle East Variome, F.S.
773 Alkuraya, J.L. Casanova, and J.G. Gleeson. 2016. Characterization of Greater Middle
774 Eastern genetic variation for enhanced disease gene discovery. *Nat Genet* 48:1071-
775 1076.
- 776 Seelow, D., M. Schuelke, F. Hildebrandt, and P. Nürnberg. 2009. HomozygosityMapper-
777 an interactive approach to homozygosity mapping. *Nucleic Acids Res* 37:W593-W599.

- 778 Seiler, C., K.C. Finger-Baier, O. Rinner, Y.V. Makhankov, H. Schwarz, S.C. Neuhaus,
779 and T. Nicolson. 2005. Duplicated genes with split functions: independent roles of
780 protocadherin15 orthologues in zebrafish hearing and vision. *Development* 132:615-
781 623.
- 782 Smith, R.J., J.F. Bale, Jr., and K.R. White. 2005. Sensorineural hearing loss in children.
783 *Lancet* 365:879-890.
- 784 Thisse, C., and B. Thisse. 2008. High-resolution in situ hybridization to whole-mount
785 zebrafish embryos. *Nat Protoc* 3:59-69.
- 786 UniProt Consortium, T. 2018. UniProt: the universal protein knowledgebase. *Nucleic*
787 *Acids Res* 46:2699.
- 788 Varshney, G.K., B. Carrington, W. Pei, K. Bishop, Z. Chen, C. Fan, L. Xu, M. Jones,
789 M.C. LaFave, J. Ledin, R. Sood, and S.M. Burgess. 2016. A high-throughput functional
790 genomics workflow based on CRISPR/Cas9-mediated targeted mutagenesis in
791 zebrafish. *Nat Protoc* 11:2357-2375.
- 792 Viotti, C. 2016. ER to Golgi-Dependent Protein Secretion: The Conventional Pathway.
793 *Methods Mol Biol* 1459:3-29.
- 794 Waterhouse, A.M., J.B. Procter, D.M. Martin, M. Clamp, and G.J. Barton. 2009. Jalview
795 Version 2--a multiple sequence alignment editor and analysis workbench. *Bioinformatics*
796 25:1189-1191.

797 Westerfield, M. 2000. The zebrafish book. A guide for the laboratory use of zebrafish
798 (*Danio rerio*). Univ. of Oregon Press, Eugene, Oregon, USA.

799 Whitfield, T.T., B.B. Riley, M.Y. Chiang, and B. Phillips. 2002. Development of the
800 zebrafish inner ear. *Dev Dyn* 223:427-458.

801 Wright, C.F., D.R. FitzPatrick, and H.V. Firth. 2018. Paediatric genomics: diagnosing
802 rare disease in children. *Nat Rev Genet* 19:253-268.

803 Xiong, H.Y., B. Alipanahi, L.J. Lee, H. Bretschneider, D. Merico, R.K. Yuen, Y. Hua, S.
804 Gueroussov, H.S. Najafabadi, T.R. Hughes, Q. Morris, Y. Barash, A.R. Krainer, N. Jojic,
805 S.W. Scherer, B.J. Blencowe, and B.J. Frey. 2015. RNA splicing. The human splicing
806 code reveals new insights into the genetic determinants of disease. *Science*
807 347:125806.

808 Yang, J., R. Yan, A. Roy, D. Xu, J. Poisson, and Y. Zhang. 2015. The I-TASSER Suite:
809 protein structure and function prediction. *Nat Methods* 12:7-8.

810

811 **Figure legends**

812 **Fig. 1. Pedigree, audiological data, genetic data, and locus mapping**

813 **(A)** The consanguineous family of Iranian origin with hearing loss and segregation of the
814 *CLRN2* c.494C>A variant.

815 **(B)** Pure-tone audiograms from affected individuals IV-1 (red) and IV-6 (blue), as well as
816 an unaffected heterozygous individual V-1 (green). Air conduction thresholds in dB HL
817 for the right and left ears are represented by circles and crosses, respectively. Bone-
818 conduction thresholds are represented by < and > for right and left ears, respectively,
819 and confirm a sensorineural hearing loss in the affected individuals.

820 **(C)** Homozygosity mapping reveals a 15.2 Mb locus on chromosome 4 containing
821 *CLRN2*.

822 **(D)** Sequence electropherograms showing the homozygous, heterozygous and WT
823 images of the *CLRN2* c.494C>A; pThr165Lys pathogenic variants.

824

825 **Fig. 2. Conservation of the p.Thr165 residue, and clarin 1/clarin 2 alignment.**

826 **(A)** Overview of clarin 2 protein and modular structure of the PMP-
827 22/EMP/EP20/Claudin superfamily, with amino acid residue coordinates and position of
828 the p.(Thr165Lys) substitution shown (upper panel). An alignment of the amino acid
829 sequences from the segment of clarin 2 (represented by dashed lines) from vertebrate
830 species shows the Thr165 position (asterisk) is well conserved among vertebrates.

831 **(B)** Alignment of clarin 2 (UniProtKB: A0PK11, upper alignment) and clarin 1
832 (UniProtKB: P58418, lower alignment) amino acid residues. Transmembrane domains

833 are marked in grey, conservation is shown in yellow, and consensus sequences are
834 shown below for the 232 amino acid proteins. Missense and nonsense variants in clarin
835 1 (Deafness Variation Database v8.2) and clarin 2 (present study, asterisk) are marked
836 in red.

837 **(C)** The predicted secondary structure of human clarin 2 (NP_001073296.1) wild-type
838 (Thr165) and mutated (Thr165Lys) protein. H represents alpha-helix, S represents beta-
839 strand and C represents coil.

840

841 **Fig. 3. Analysis of the *CLRN2* c.494C>A variant on splicing**

842 **(A)** Schematic illustration of the mini-gene splice construct design. Genomic
843 representation of *CLRN2*, including the position of the missense variant c.494C>A
844 (arrow) on exon 3 with 3' UTR (green), and the 5' UTR, as well as exons 1 and 2 (grey)
845 (upper panel). Regions captured by mini-gene PCR primers are represented in green.
846 Schematic illustration of the mini-gene splice construct including exon 3 and its flanking
847 sequence (green) cloned into multiple cloning sites (*Sal*I and *Sac*II sites) of pET01
848 backbone vector (lower panel). Blue boxes represent native exons of the pET01 vector.

849 **(B)** RT-PCR of transcripts from post-mini-gene transfected COS-7 cells. Amplicons
850 derived from the transcripts of WT (*CLRN2*), a benign *CLRN2* polymorphism
851 (rs117875715, chr4(GRCh37):g.17,528,480G>A), the *CLRN2* c.494C>A variant and a
852 negative control, were visualized on a 1.5% agarose gel. The SNP, rs117875715, was
853 used to test and validate the designed WT and mutant mini-gene assay. The ~650 bp
854 amplicon was associated with the WT and validation control rs117875715. The

855 amplicon derived from the *CLRN2* c.494C>A transcripts showed two bands: a 650 bp
856 band and a larger ~1360 bp band, indicating retention of intron separating the donor site
857 of the 5' exon and the acceptor site of *CLRN2* exon 3.

858 **(C)** Retention of intron in *CLRN2* c.494C>A mini-gene results in a stop codon (TGA)
859 after *CLRN2* exon 2.

860

861 **Fig. 4. Clarin 2 is required for the inner ear function in zebrafish**

862 **(A)** RT-qPCR of *clrn2* mRNA expression from 1 to 120 hpf of WT embryos/larvae. *clarin*
863 2 mRNA expression can be detected starting from 18 hpf and then increased
864 throughout development. The bar graphs showed the mean values \pm SEM after
865 normalization to the housekeeping gene *18S* level and then compared to 18 hpf.

866 **(B)** RT-qPCR of *clrn2* mRNA expression in different adult tissues. The bar graphs
867 displayed mean values \pm SEM after normalization to the housekeeping gene *18S* level
868 and then compared to muscle.

869 **(C, D)** Whole-mount in situ hybridization (WISH) using antisense *clrn2* probe reveals the
870 inner ear expression of *clrn2* mRNA (relative dark purple color, black arrowhead) at 3
871 (C) and 5 (D) dpf embryos. Sense *clrn2* probe was used as negative control and relative
872 light purple color is considered as background. *clrn2* mRNA was consistently expressed
873 in hair cells within inner ear macula (C, D) with lined and arrayed structure. A known
874 hair cell marker *pvalb9* was used as an indicator for hair cells in the inner ear of 3 dpf
875 embryos (C). Cryosection was performed after *clrn2* WISH at 5 dpf to confirm the small

876 patch of signal on the macula is hair cells rather than supporting cells (D, black arrow
877 middle panel). Scale bar = 100 μm , except middle panel in D (20 μm).

878

879 **(E)** RT-qPCR of *clrn2* mRNA expression level was decreased 70% in *clrn2* crispants
880 compared to uninjected larvae, indicating *clrn2* was successfully knocked out (E, upper
881 panels). Phalloidin staining on *clrn2* crispants show that the hair cells in the inner ear
882 macula display splayed, thin and split structures (red arrowhead in lower panels). Scale
883 bar = 10 μm .

884

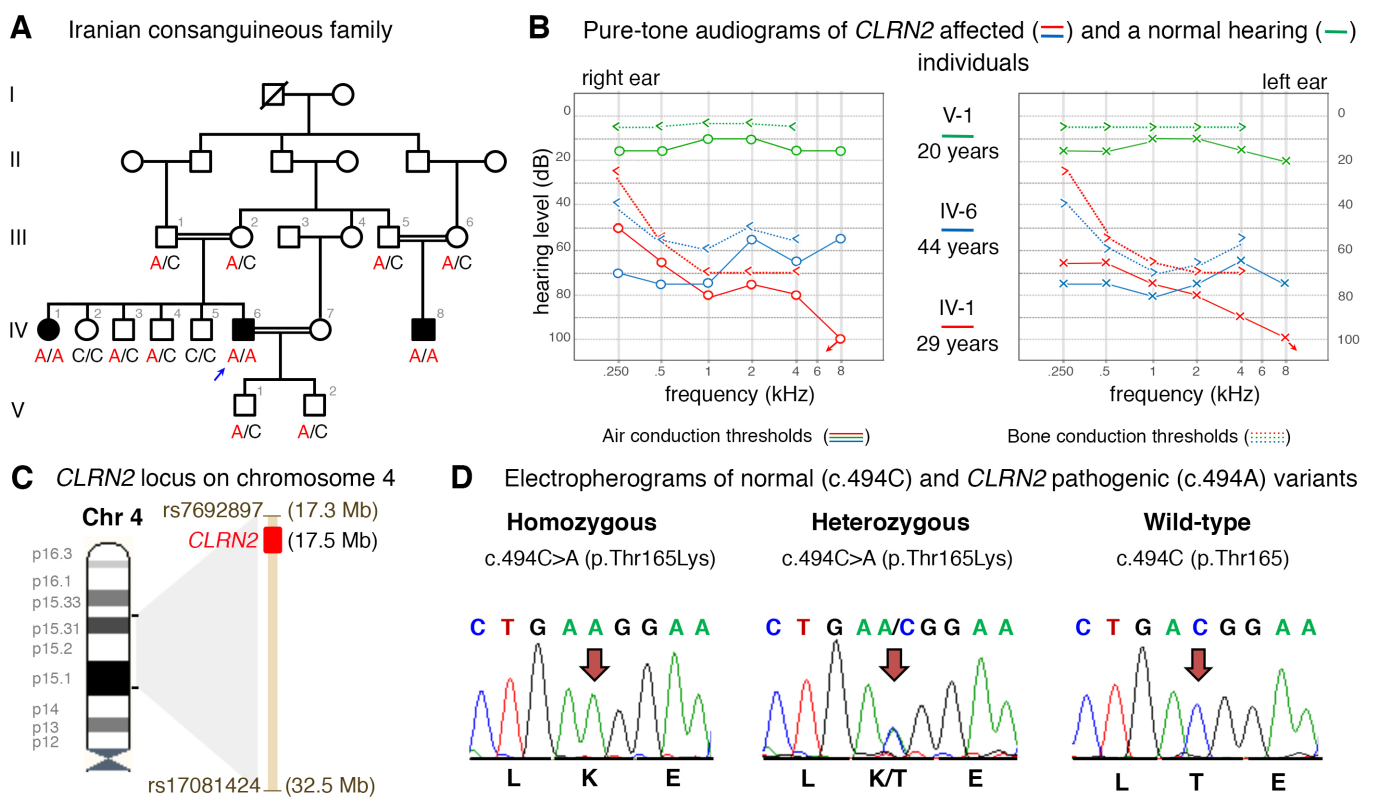
885 **Figure 5. Clarin 2 is required for hearing function in mouse**

886 **(A)** The genomic structure of mouse *Clrn2* (ENSMUST00000053250), and domains of
887 the encoded tetraspan-like glycoprotein (232 amino acids). The positions of the
888 transmembrane (TM) domains (dark green) and the structures of the WT *Clrn2* and
889 *Clrn2*^{del629} alleles are indicated.

890 **(B)** ABR threshold measurements at P21 (\pm 1 day) show that *Clrn2*^{del629/del629} mice (red)
891 exhibit a severe-to-profound hearing loss affecting all frequencies tested, with
892 thresholds at 80 dB SPL and beyond. Age-matched *Clrn2*^{+/+} (black) and *Clrn2*^{del629/+}
893 (grey) controls display thresholds within the expected range (15-40 dB SPL). Data
894 shown are mean \pm SD. *** p <0.001, one-way ANOVA. **(C)** Averaged DPOAE responses
895 at P28 (\pm 1 day), showing significantly reduced responses in *Clrn2*^{del629/del629} mice. Data
896 shown are mean \pm SD. * p <0.02, ** p <0.01, one-way ANOVA.

897 **(C)** Pseudo-colored scanning electron micrographs illustrate the three full rows, tallest
898 (red), middle (blue) and short (yellow), of P28 (\pm 1 day) stereocilia in IHC and OHC hair
899 bundles. Unlike the fragmented hair bundle in *Cln1*^{-/-} mice, lack of clarin-2 does not
900 affect the shape of IHC or OHC hair bundles. However, all the short row stereocilia have
901 completely or partially regressed in the absence of either clarin protein.

902 Scale bar = 1 μ m.



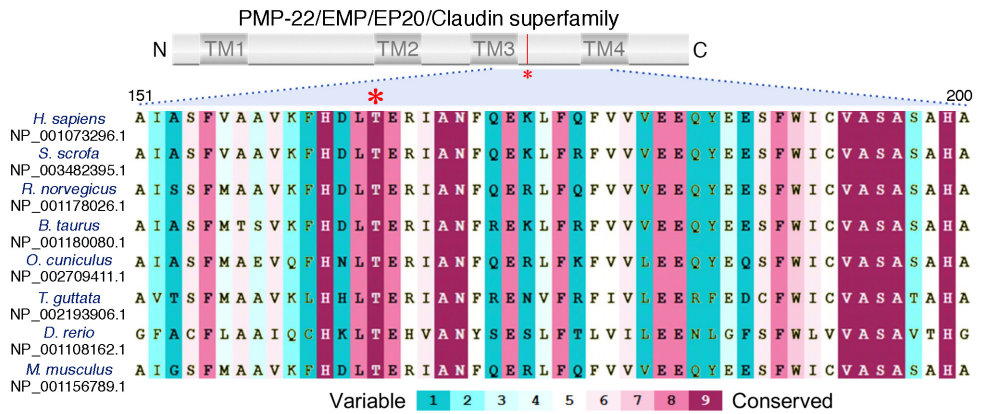
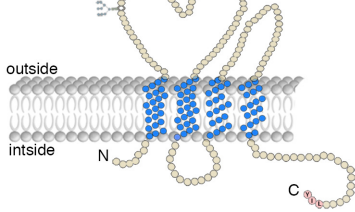
A The tetraspan-like clarin proteins

Glycosylation at asparagine:

in Clarin 1 and Clarin 2: N48

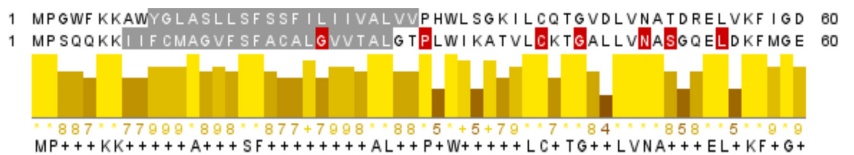
in Clarin 3: N83

in PMP-22: N41



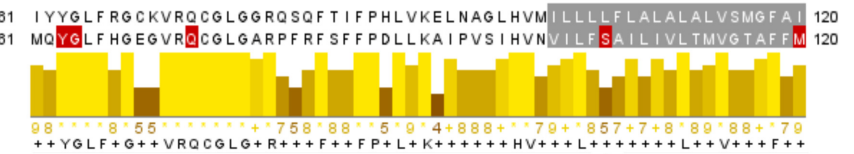
B *CLRN2* *H. sapiens* (aa 1-232; *SP/A0PK11*)
CLRN1 *H. sapiens* (aa 1-232; *SP/P58418*)

conservation



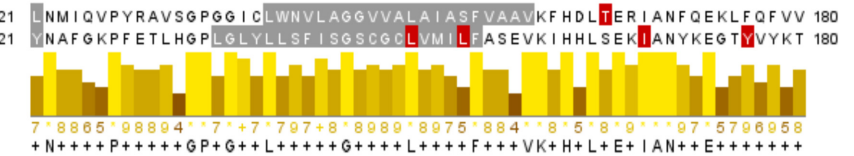
CLRN2 *H. sapiens* (aa 1-232; *SP/A0PK11*)
CLRN1 *H. sapiens* (aa 1-232; *SP/P58418*)

conservation



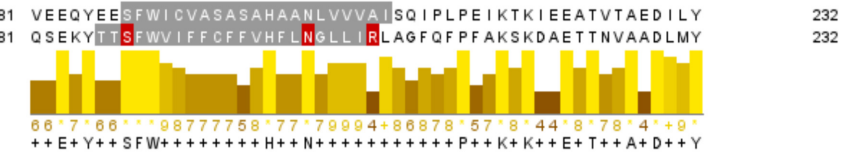
CLRN2 *H. sapiens* (aa 1-232; *SP/A0PK11*)
CLRN1 *H. sapiens* (aa 1-232; *SP/P58418*)

conservation

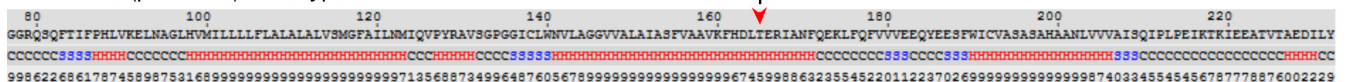


CLRN2 *H. sapiens* (aa 1-232; *SP/A0PK11*)
CLRN1 *H. sapiens* (aa 1-232; *SP/P58418*)

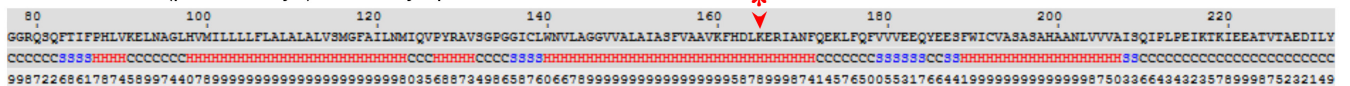
conservation

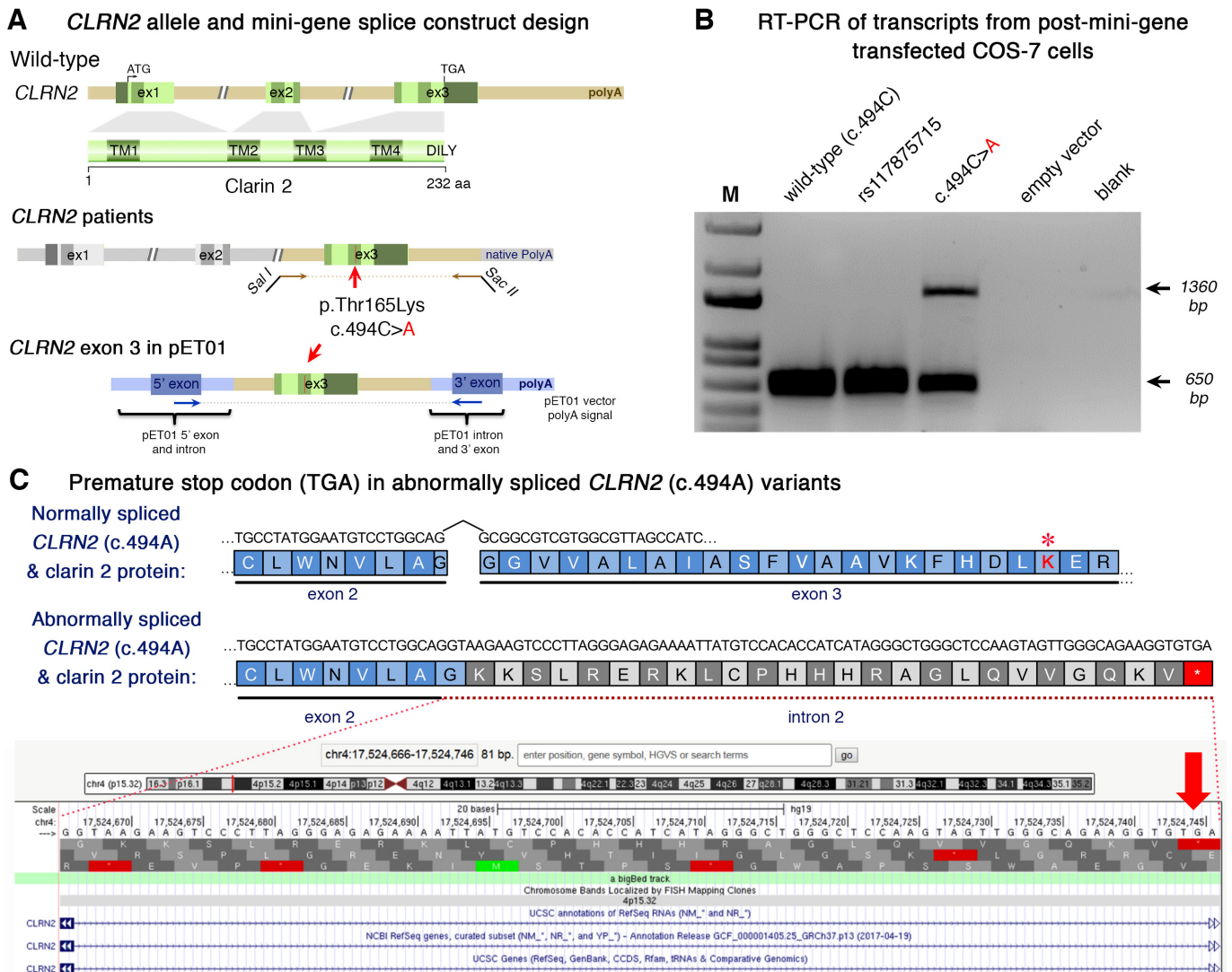


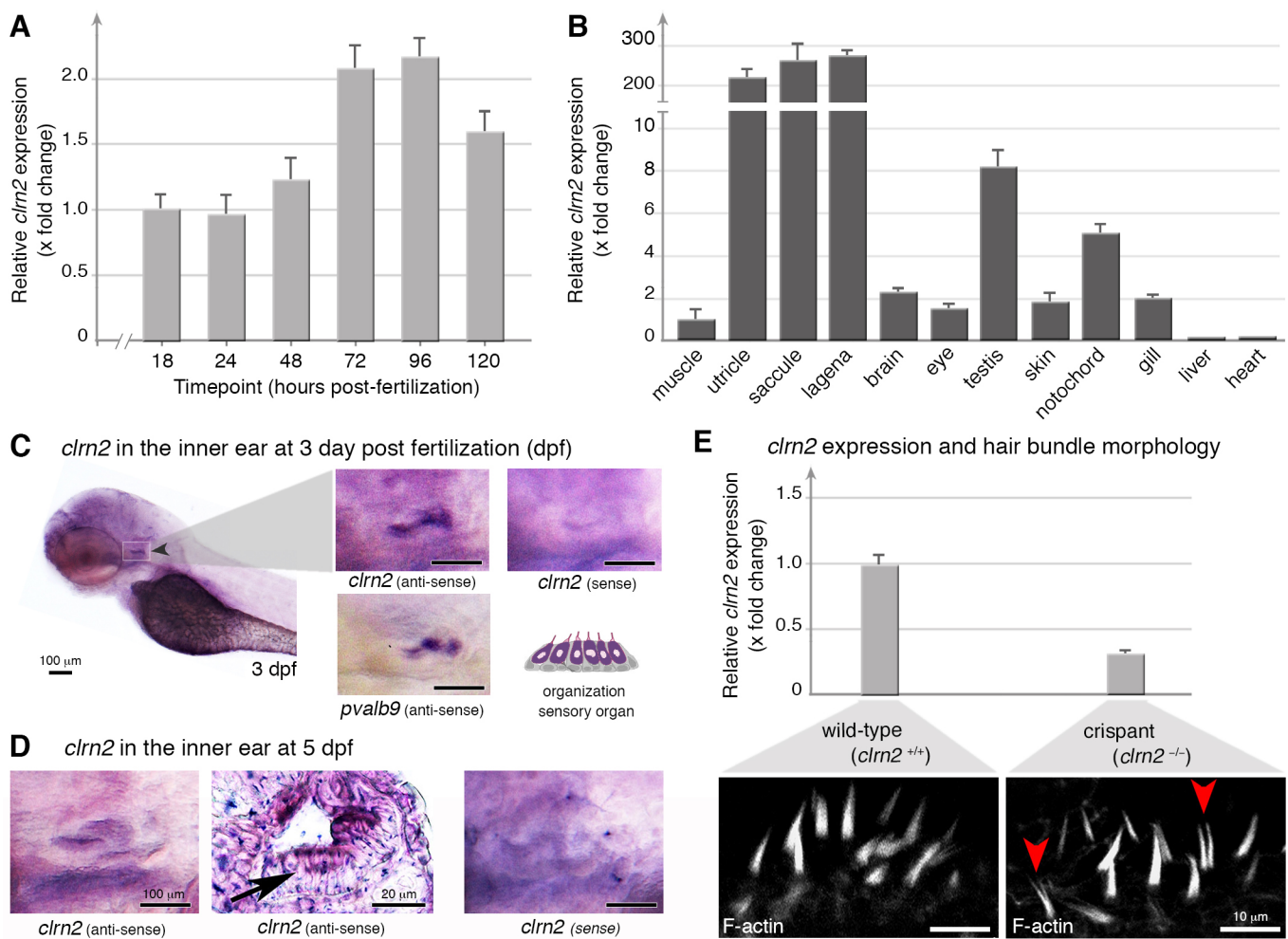
C Clarin 2 (p.Thr165): wild type



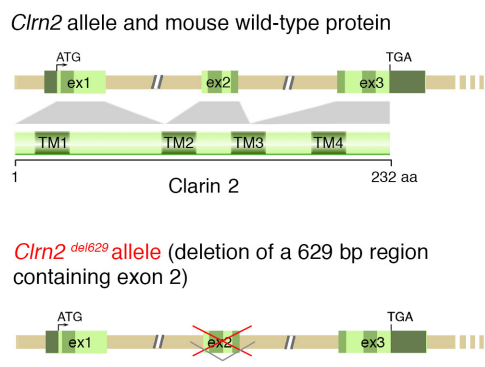
Mutant Clarin 2 (p.Thr165Lys): normally spliced variant



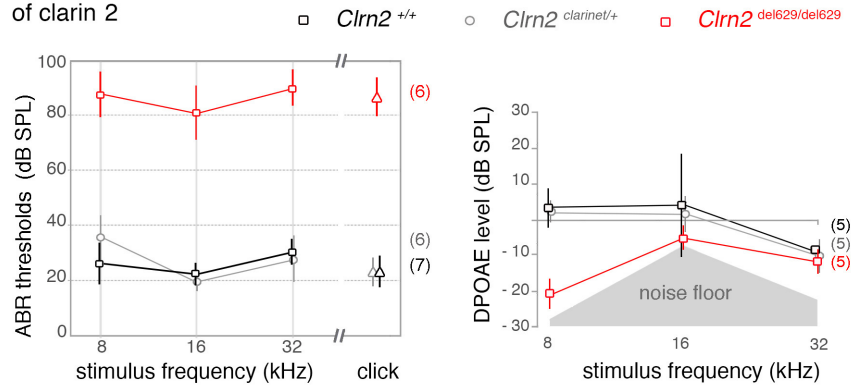




A *Cln2* in wild-type and mutant mice



B ABR thresholds and DPOAEs in presence (□, ○) or absence (◻, ◯) of clarin 2



C Loss of short row stereocilia in *Cln2*-deficient hair bundles

